HHT-alpha and TR-BDF2 schemes for Nitsche-based discrete dynamic contact

Hao Huang, Nicolas Pignet, Franz Chouly

HHT-α and TR-BDF2 schemes for Nitsche-based discrete dynamic contact

Hao HUANG[0009−0006−8471−4263], Nicolas PIGNET[0000−0001−9010−9007], and Franz CHOULY[0000−0002−9087−3301]

Abstract This study investigates the computational efficacy of HHT-α and TR-BDF2 schemes in addressing dynamic frictionless unilateral contact challenges between an elastic structure and a rigid obstacle. The application of combinations of Nitsche's method with these schemes is explored for managing unilateral contact conditions. An examination of the convergence behavior involving the parameter α in the HHT-α method is conducted. Additionally, the mass redistribution method is tested and compared against the standard mass matrix. The numerical outcomes, based on 1D and 3D benchmarks, demonstrate the effectiveness of the employed combinations of schemes and methods.

1 Introduction

The finite element method is crucial in computational solid mechanics, particularly for contact problems in the industrial sector. These problems often face issues with parasitic oscillations and energy conservation. Nonlinear boundary conditions in displacement fields are a primary challenge, addressed through weak formulation using variational inequalities, which form the foundational basis of most Finite Element Methods (FEM). Current methods for discretizing contact conditions include penal-

Hao HUANG
EDF, 7 boulevard Gaspard Monge, 91120 Palaiseau, France
Institut de Mathématiques de Bourgogne, Université de Bourgogne Franche-Comté, 21078 Dijon, France, e-mail: hao.olivier.huang@gmail.com

Nicolas, PIGNET
EDF, e-mail: nicolas.pignet@edf.fr

Franz CHOULY
CI^{2}MA, Universidad de Concepción, Concepción, Chile
CMM, University of Chile, Santiago, Chile, e-mail: franz.chouly@gmail.com

ization, mixed/mortar methods, Nitsche's method, and the augmented Lagrangian method. The field anticipates advancements in simulation accuracy and robustness.

Discretization choices involve selecting the finite element space, enforcing contact conditions, and deciding on a time-stepping scheme. Nitsche's method, initially for Dirichlet boundary conditions [11], is now applied to contact problems, offering a semi-discrete, energy-conserving approach in space-time dynamics [2, 3, 4, 6]. The HHT-α [8] and TR-BDF2 schemes [1] are prominent for time integration in dynamic problems, with the latter gaining interest for nonlinear cases.

This research explores the dynamics of frictionless impact between elastic bodies and rigid obstacles, focusing on integrating time-marching schemes with Nitsche's method. It aims to assess the effects of numerical parameters, the emergence of parasitic oscillations, and energy preservation in simulations, thereby enhancing accuracy and stability in non-regular dynamic problems.

2 Dynamic contact problems via Nitsche's method

We examine an elastic body denoted as $\Omega \subset \mathbb{R}^d$, where $d \in 1, 2, 3$. The boundary $\partial\Omega$ comprises Dirichlet, Neumann, and Signorini boundary conditions on disjoint subsets Γ_D, Γ_N, and Γ_C.

We seek the displacement field $\mathbf{u} : \Omega \times (0,T) \to \mathbb{R}^d$, for $T > 0$, governed by equations (1):

$$
\begin{aligned}
\rho\ddot{\mathbf{u}} - \operatorname{div}(\sigma(\mathbf{u})) &= \mathbf{f}, \ \text{in } \Omega \times (0,T), && \text{(i)}\\
\sigma(\mathbf{u}) = \lambda\, \operatorname{tr}(\epsilon(\mathbf{u}))\mathbf{I} + 2\mu\epsilon(\mathbf{u}), &\ \text{in } \Omega \times (0,T), && \text{(ii)}\\
\mathbf{u} &= \mathbf{0}, \ \text{on } \Gamma_D \times (0,T), && \text{(iii)}\\
\sigma(\mathbf{u}) \cdot \mathbf{n} &= \mathbf{f}_N, \ \text{on } \Gamma_N \times (0,T), && \text{(iv)}\\
u_n \le 0, \quad \sigma_n(\mathbf{u}) \le 0, \quad u_n\sigma_n(\mathbf{u}) &= 0, \ \text{on } \Gamma_C \times (0,T), && \text{(v)}\\
\sigma(\mathbf{u}) \cdot \mathbf{n} - \sigma_n(\mathbf{u}) \cdot \mathbf{n} &= \mathbf{0}, \ \text{on } \Gamma_C \times (0,T), && \text{(vi)}\\
\mathbf{u}(\cdot,0) = \mathbf{u}_0, \quad \dot{\mathbf{u}}(\cdot,0) &= \dot{\mathbf{u}}_0, \ \text{in } \Omega. && \text{(vii)}
\end{aligned}
\tag{1}
$$

The following physical parameters and terms are involved in equations (i) - (iv): mass density ρ, source terms $\mathbf{f}$, $\mathbf{f}_N$, Lamé coefficients λ, μ, and deformation tensor $\epsilon(\cdot)$. Equations (v) and (vi) define Signorini's conditions in frictionless case, with $u_n = \mathbf{u} \cdot \mathbf{n}$ and $\sigma_n(\mathbf{u}) = (\sigma(\mathbf{u}) \cdot \mathbf{n}) \cdot \mathbf{n}$. Equation (vii) sets initial conditions.

The displacement is discretized using the Lagrange finite element space $\mathbf{V}^h$, which is of degree one or two ($k = 1$ or 2), and is constructed based on a mesh $\mathcal{T}^h$ of the domain Ω:

$$
\mathbf{V}^h := \left\{ \mathbf{v}^h \in \left(C^0(\overline{\Omega})\right)^d : \mathbf{v}^h_{|\Gamma_D} = \mathbf{0};\ \mathbf{v}^h_{|T} = \mathbb{P}_k(T),\ \forall T \in \mathcal{T}^h \right\}. \tag{2}
$$

We also define the bilinear and linear forms $a(\mathbf{u},\mathbf{v}) := (\sigma(\mathbf{u}),\epsilon(\mathbf{v}))_\Omega$ and $l(\mathbf{v}) := (\mathbf{f},\mathbf{v})_\Omega + (\mathbf{f}_N,\mathbf{v})_{\Gamma_N}$ using L^2-products $(\mathbf{u},\mathbf{v})_\Omega := \int_\Omega \mathbf{u}\cdot\mathbf{v}\,\mathrm{d}\Omega$ and $(\mathbf{u},\mathbf{v})_{\Gamma_F} := \int_{\Gamma_F}\mathbf{u}\cdot\mathbf{v}\,\mathrm{d}\Gamma$, defined on Ω and Γ_F respectively, with $\Gamma_F \in \{\partial\Omega,\Gamma_D,\Gamma_N,\Gamma_C\}$. The norm used in the following is denoted by $||\cdot||_\Omega := (\cdot,\cdot)_\Omega^{\frac{1}{2}}$ and $||\cdot||_{\Gamma_F} := (\cdot,\cdot)_{\Gamma_F}^{\frac{1}{2}}$.

The total mechanical energy associated with the solution $\mathbf{u}$ of the dynamic Signorini problem is given by:

$$E(t) = \frac{1}{2}(\rho\dot{\mathbf{u}},\dot{\mathbf{u}})_\Omega + \frac{1}{2}a(\mathbf{u},\mathbf{u}),\ \forall t\in[0,T]. \tag{3}$$

Additionally, by the persistency condition [7], which states that $(\sigma(\mathbf{u})\cdot\mathbf{n})\cdot\dot{\mathbf{u}} = 0$ on Γ_C, and when the linear form l is null, the evolution of energy $\frac{d}{dt}E(t) = 0$ implies that the total mechanical energy remains constant over time.

The semi-discrete reformulation of Nitsche's method is as follows:

$$\begin{cases}\text{Seek } \mathbf{u}^h : [0,T]\to\mathbf{V}^h,\ \text{s.t.}\\ \left(\rho\ddot{\mathbf{u}}^h(t),\mathbf{v}^h\right)_\Omega + a_{\gamma_N}(\mathbf{u}^h(t),\mathbf{v}^h) + \left(\frac{1}{\gamma_N}\left[P_N(\mathbf{u}^h(t))\right]_{\mathbb{R}^-},P_N(\mathbf{v}^h)\right)_{\Gamma_C} = l(\mathbf{v}),\ \forall\mathbf{v}^h\in\mathbf{V}^h,\end{cases} \tag{4}$$

with $[\cdot]_{\mathbb{R}^-} := \min(0,\cdot)$, $a_{\gamma_N}(\mathbf{u}^h,\mathbf{v}^h) := a(\mathbf{u}^h,\mathbf{v}^h) - \left(\frac{1}{\gamma_N}\sigma_n(u^h),\sigma_n(v^h)\right)_{\Gamma_C}$ and the linear discrete operator P_N defined as:

$$P_N : \begin{array}{l}\mathbf{V}^h\to L^2(\Gamma_C)\\ \mathbf{v}^h\mapsto \sigma_n(\mathbf{v}^h) - \gamma_N v_n^h,\end{array} \tag{5}$$

with γ_N being a positive function $\gamma_{N|T\cap\Gamma_C} = \frac{\gamma_0}{h_T}$.

The compact form of this Lipschitz system can be written as:

$$\begin{cases}\text{Seek } \mathbf{u}^h : [0,T]\to\mathbf{V}^h,\ \text{s.t.}\\ \mathbf{M}(\ddot{\mathbf{u}}^h(t)) + \mathbf{B}_N(\mathbf{u}^h(t)) = \mathbf{L}(t),\\ \mathbf{u}^h(0) = \mathbf{u}_0^h,\quad \dot{\mathbf{u}}^h(0) = \dot{\mathbf{u}}_0^h,\end{cases} \tag{6}$$

where the operators $\mathbf{M} : \mathbf{V}^h\to\mathbf{V}^h$ and $\mathbf{B}_N : \mathbf{V}^h\to\mathbf{V}^h$ are defined such that

$$\begin{aligned}&\left(\mathbf{M}(\mathbf{v}^h),\mathbf{w}^h\right)_\Omega = \left(\rho\mathbf{v}^h,\mathbf{w}^h\right)_\Omega,\ \forall\mathbf{w}^h\in\mathbf{V}^h,\\ &\left(\mathbf{B}_N(\mathbf{v}^h),\mathbf{w}^h\right) = a_{\gamma_N}(\mathbf{v}^h,\mathbf{w}^h) + \left(\frac{1}{\gamma_N}\left[P_N(\mathbf{v}^h)\right]_{\mathbb{R}^-},P_N(\mathbf{w}^h)\right)_{\Gamma_C},\ \forall\mathbf{w}^h\in\mathbf{V}^h,\end{aligned} \tag{7}$$

and the vector $\mathbf{L}(t)\in\mathbf{V}^h$ is defined such that $\left(\mathbf{L}(t),\mathbf{w}^h\right)_\Omega = l(\mathbf{w}^h),\ \forall\mathbf{w}^h\in\mathbf{V}^h$.

The discrete energy, denoted as $E^h(t)$, can be set in the following manner: $E^h(t) := \frac{1}{2}\left(\rho\dot{\mathbf{u}}^h(t),\dot{\mathbf{u}}^h(t)\right)_\Omega + \frac{1}{2}a(\mathbf{u}^h(t),\mathbf{u}^h(t))$,

It essentially mirrors the mechanical energy $E(t)$ within a continuous framework. Furthermore, we introduce a modified energy associated to the system:

$$
\begin{aligned}
E_N^h(t) &:= E^h(t) - \frac{1}{2}\left\|\gamma_N^{-\frac{1}{2}}\sigma_n(\mathbf{u}^h(t))\right\|_{\Gamma_C}^2 + \frac{1}{2}\left\|\gamma_N^{-\frac{1}{2}}\left[\mathbb{P}_N(\mathbf{u}^h(t))\right]_{\mathbb{R}^-}\right\|_{\Gamma_C}^2 \\
&:= E^h(t) - R_N^h(t),
\end{aligned} \tag{8}
$$

The term $R_N^h(t)$, in a broader sense, reflects the deviation from the contact condition (1)(v) by $\mathbf{u}^h(t)$, as discussed in [3]. This revised energy expression, E_N^h, is preserved under the assumption that (1) is conservative.

3 Time-marching schemes

The two time-marching schemes under consideration in this work are HHT-α [8] and TR-BDF2 [1] schemes. Here we use a uniform discretization of the time interval $[0, T]$ with time-step Δt, and $t^n = n\Delta t, n = 0, \cdots, N$. The schemes consist of solving a nonlinear problem for each time instant t^{n+1} using the displacement $\mathbf{u}^{h,n}$, velocity $\dot{\mathbf{u}}^{h,n}$, and acceleration $\ddot{\mathbf{u}}^{h,n}$ of instant t^n as known variables. For HHT-α and TR-BDF2 schemes, the nonlinear problems to be solved are respectively (9) and (10).

$$
\begin{cases}
\text{Seek } \mathbf{u}^{h,n+1}, \dot{\mathbf{u}}^{h,n+1}, \ddot{\mathbf{u}}^{h,n+1} \in \mathbf{V}^h \text{ s.t.} & \\
\mathbf{u}^{h,n+1} = \mathbf{u}^{h,n} + \Delta t\dot{\mathbf{u}}^{h,n} + \dfrac{\Delta t^2}{2}((1-2\tilde{\beta})\ddot{\mathbf{u}}^{h,n} + 2\tilde{\beta}\ddot{\mathbf{u}}^{h,n+1}), & \text{(i)} \\
\dot{\mathbf{u}}^{h,n+1} = \dot{\mathbf{u}}^{h,n} + \Delta t((1-\tilde{\gamma})\ddot{\mathbf{u}}^{h,n} + \tilde{\gamma}\ddot{\mathbf{u}}^{h,n+1}), & \text{(ii)} \\
\mathbf{M}\ddot{\mathbf{u}}^{h,n+1} + (1-\tilde{\alpha})\mathbf{B}(\mathbf{u}^{h,n+1}) + \tilde{\alpha}\mathbf{B}(\mathbf{u}^{h,n}) = (1-\tilde{\alpha})\mathbf{L}^{n+1} + \tilde{\alpha}\mathbf{L}^n, & \text{(iii)}
\end{cases} \tag{9}
$$

$$
\begin{cases}
\text{Seek } \mathbf{u}^{h,n+1}, \dot{\mathbf{u}}^{h,n+1}, \ddot{\mathbf{u}}^{h,n+1} \in \mathbf{V}^h \text{ s.t.} & \\
\tilde{\dot{\mathbf{u}}}^{h,n+\tilde{\mu}} = \dot{\mathbf{u}}^{h,n} + \dfrac{\tilde{\mu}\Delta t}{2}\left(\ddot{\mathbf{u}}^{h,n} + \tilde{\ddot{\mathbf{u}}}^{h,n+\tilde{\mu}}\right), & \text{(i)} \\
\tilde{\mathbf{u}}^{h,n+\tilde{\mu}} = \mathbf{u}^{h,n} + \tilde{\mu}\Delta t\dot{\mathbf{u}}^{h,n} + \dfrac{\tilde{\mu}^2\Delta t^2}{4}\left(\ddot{\mathbf{u}}^{h,n} + \tilde{\ddot{\mathbf{u}}}^{h,n+\tilde{\mu}}\right), & \text{(ii)} \\
\mathbf{M}\tilde{\ddot{\mathbf{u}}}^{h,n+\tilde{\mu}} + \mathbf{B}(\tilde{\mathbf{u}}^{h,n+\tilde{\mu}}) = \mathbf{L}^{n+\tilde{\mu}}, & \text{(iii)} \\
\dot{\mathbf{u}}^{h,n+1} = \dfrac{1}{\tilde{\mu}(2-\tilde{\mu})}\tilde{\dot{\mathbf{u}}}^{h,n+\tilde{\mu}} - \dfrac{(1-\tilde{\mu})^2}{\tilde{\mu}(2-\tilde{\mu})}\dot{\mathbf{u}}^{h,n} + \dfrac{1-\tilde{\mu}}{2-\tilde{\mu}}\Delta t\ddot{\mathbf{u}}^{h,n+1}, & \text{(iv)} \\
\mathbf{u}^{h,n+1} = \dfrac{1}{\tilde{\mu}(2-\tilde{\mu})}\tilde{\mathbf{u}}^{h,n+\tilde{\mu}} - \dfrac{(1-\tilde{\mu})^2}{\tilde{\mu}(2-\tilde{\mu})}\mathbf{u}^{h,n} + \dfrac{1-\tilde{\mu}}{2-\tilde{\mu}}\Delta t\dot{\mathbf{u}}^{h,n+1}, & \text{(v)} \\
\mathbf{M}\ddot{\mathbf{u}}^{h,n+1} + \mathbf{B}(\mathbf{u}^{h,n+1}) = \mathbf{L}^{n+1}. & \text{(vi)}
\end{cases} \tag{10}
$$

The scheme parameters $(\tilde{\alpha}, \tilde{\beta}, \tilde{\gamma})$ for the HHT-α scheme are often interrelated. Typically, $\tilde{\alpha} \in [0, \frac{1}{3}]$, $\tilde{\beta} = \frac{1}{4}(1+\tilde{\alpha})^2$, and $\tilde{\gamma} = \frac{1}{2} + \tilde{\alpha}$, ensuring unconditional sta-

bility for linear elasticity in an implicit scheme. The Crank-Nicolson scheme, or the Newmark family's implicit trapezoidal method, arises when $\tilde{\alpha} = 0$, $\tilde{\beta} = \frac{1}{4}$, and $\tilde{\gamma} = \frac{1}{2}$, providing second-order accuracy and energy conservation in linear elasticity without contact. However, contact can introduce oscillations and perturbation of numerical energy, especially with the Crank-Nicolson scheme [10]. Higher $\tilde{\alpha}$ values can reduce high-frequency oscillations but may also lead to significant energy dissipation, challenging industrial reliability. A negative value for the parameter $\tilde{\alpha}$ (with $\tilde{\beta} = \frac{1}{4}(1 + |\tilde{\alpha}|)^2$ and $\tilde{\gamma} = \frac{1}{2} + |\tilde{\alpha}|$ to keep the values of $\tilde{\beta}$ and $\tilde{\gamma}$ remaining in the unconditionally stable region) can also provide a convergence form and dissipate high-frequency oscillations [9].

The TR-BDF2 scheme, recognized as an L-stable predictor-corrector approach, employs the implicit trapezoidal rule (Crank-Nicolson) for the predictor with a step size of $\tilde{\mu}\Delta t$. The scheme then applies the second-order backward differentiation formula for the corrector, leveraging data from t^n and the outcomes of the predictor. For linear elasticity, an interesting value for $\tilde{\mu}$ is $2 - \sqrt{2}$, which makes the linear systems at both sub-steps identical. In this work, we also use this value $\tilde{\mu} = 2 - \sqrt{2}$ of the parameter even though, for the non-linear case, the two sub-steps are solved by Newton iteration with different initial values.

4 Numerical results

In this work, we investigate the performance of the combination of Nitsche's method and two time-marching schemes by solving the movement of a 1D elastic bar of length 1 with two Signorini boundary conditions (at $x = 0$ and $x = 1.5$), using P_1 finite elements. GetFEM [12] via Python interface was used for the simulations in this work.

$$\begin{cases} \text{Seek } u(x,t) : [0,1] \times (0,T) \to \mathbb{R}, \text{ s.t.} \\ \dfrac{\partial^2 u}{\partial t^2} - \dfrac{\partial^2 u}{\partial x^2} = 0, \\ u(0,t) \geq 0,\ \dfrac{\partial u}{\partial x}(0,t) \leq 0,\ u(0,t)\dfrac{\partial u}{\partial x}(0,t) = 0, \\ u(1,t) \leq \dfrac{1}{2},\ \dfrac{\partial u}{\partial x}(1,t) \leq 0,\ \left(u(1,t) - \dfrac{1}{2}\right)\dfrac{\partial u}{\partial x}(1,t) = 0, \\ u(x,0) = 1 - \dfrac{x}{2},\ \dfrac{\partial u}{\partial t}(x,0) = -\dfrac{1}{2}. \end{cases} \tag{11}$$

The analytical solution exhibits piecewise regularity and periodicity. The $x - t$ diagram in Figure 1 visualizes the analytical solution by demonstrating the time-varying displacement. The bar's interaction with each side manifests in three distinct states: non-contact, contact with zero contact pressure, and contact with nonzero contact pressure. The benchmark's critical focus is the second state, where contact occurs without pressure, especially notable at $x = 0$ for $t \in [1, 2]$. This scenario,

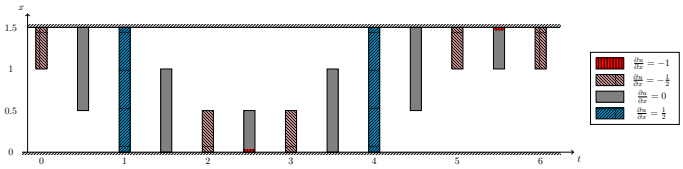

Fig. 1: Elastic bar with two Signorini boundary conditions.

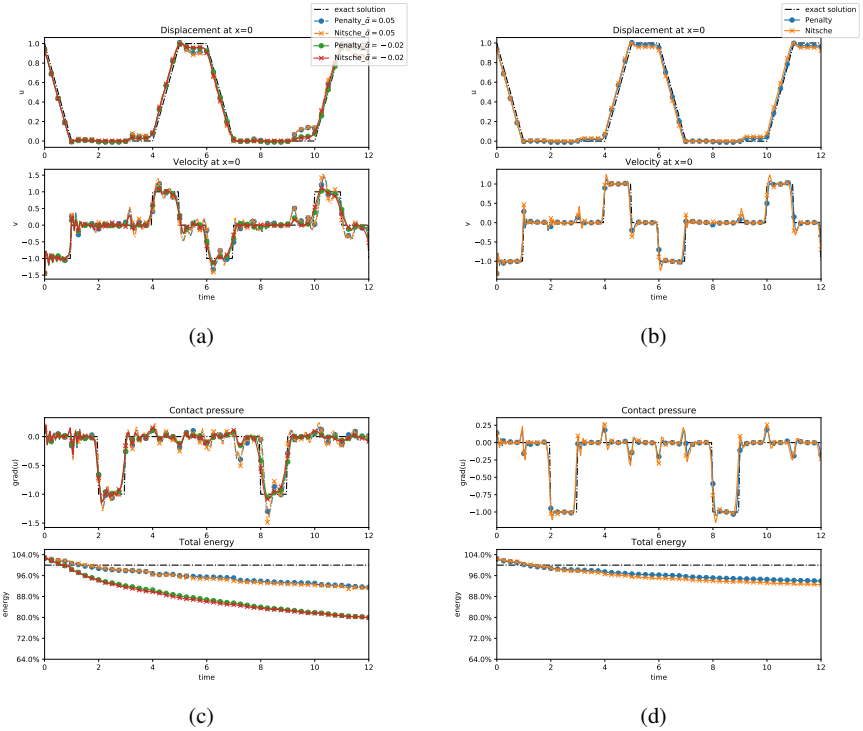

Fig. 2: Comparison of the analytical and discrete solutions (Nitsche's and penalty methods) for the HHT-α, $\tilde{\alpha} \in \{0.05, -0.02\}$ (left) and TR-BDF2 (right) schemes.

termed "grazing contact" – characterized by both zero normal displacement ($u_n = 0$) and zero gradient ($\frac{\partial u}{\partial x} = 0$) on the contact boundary Γ_C – represents a non-differentiable case for the operators $\mathbf{B}_N$, as mentioned in [5].

For the simulation, both mesh size and time step are consistently set to $h = 0.05$ and $\Delta t = 0.05$, respectively. We compare the numerical results of Nitsche's method with those of the penalty method with the formulation presented in [9, Sec. 2.2]. The Nitsche parameter γ_0 and the penalty parameter ϵ_0 are chosen to be equal, with $\gamma_0 = \frac{1}{\epsilon_0} = 5$.

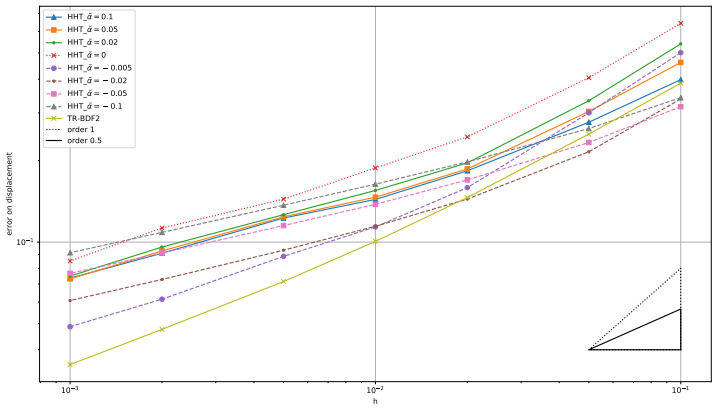

Fig. 3: L^2H^1-error vs h with $\frac{\Delta t}{h} = 1$.

Table 1: numerical cost for different schemes

Crank-Nicolson	HHT-α ($\tilde{\alpha} = 0.05$)	TR-BDF2
0.9358 s	0.8907 s	1.4585 s

According to the numerical results presented in Fig. 2, our observations lead to several noteworthy insights. By applying various mesh sizes and time steps with a fixed ration $\frac{\Delta t}{h} = 1$, we show the errors on $L^2(0,T;H^1(\Omega))$-norm in Fig. 3. The orders of convergence are similar and close to $\frac{1}{2}$. Table 1 also displays the CPU times consumed by Crank-Nicolson (HHT-α with $\tilde{\alpha} = 0$), HHT-α with $\tilde{\alpha} = 0.05$ and TR-BDF2 schemes on a computer equipped with an Intel® Core™ i7-9850H CPU.

Nitsche's method shows superior compliance with contact conditions, outperforming the penalty method due to its inherent consistency. For balancing energy loss and spurious oscillations, the HHT-α method, particularly with a negative and small absolute value of α, emerges as a viable option. On the other hand, the TR-BDF2 scheme offers an attractive balance between energy conservation and oscillation reduction, albeit at a higher computational cost compared to HHT-α schemes. Notably, in scenarios involving very fine time steps, the HHT-α method may prove more advantageous due to its lower cost and reduced dissipation of high frequencies. While not covered in this work, the mass redistribution method, when combined with the TR-BDF2 scheme, could exhibit promising behavior, especially concerning contact pressure. For further insights and detailed analyses, readers are encouraged to consult [9].

Acknowledgements FC thanks the CMM grant FB20005.

References

1. K. J. Bathe and M. M. I. Baig. On a composite implicit time integration procedure for nonlinear dynamics. *Computers & Structures*, 83(31-32):2513–2524, 2005.
2. F. Chouly and P. Hild. A Nitsche-based method for unilateral contact problems: numerical analysis. *SIAM Journal on Numerical Analysis*, 51(2):1295–1307, 2013.
3. F. Chouly, P. Hild, and Y. Renard. A Nitsche finite element method for dynamic contact: 1. Space semi-discretization and time-marching schemes. *ESAIM: Mathematical Modelling and Numerical Analysis*, 49(2):481–502, 2015.
4. F. Chouly, P. Hild, and Y. Renard. A Nitsche finite element method for dynamic contact: 2. Stability of the schemes and numerical experiments. *ESAIM: Mathematical Modelling and Numerical Analysis*, 49(2):503–528, 2015.
5. F. Chouly, P. Hild, and Y. Renard. Symmetric and non-symmetric variants of Nitsche's method for contact problems in elasticity: theory and numerical experiments. *Mathematics of Computation*, 84(293):1089–1112, 2015.
6. F. Chouly, P. Hild, and Y. Renard. *Finite element approximation of contact and friction in elasticity*, volume 48 of *Advances in Mechanics and Mathematics / Advances in Continuum Mechanics*. Birkhäuser, Springer, 2023. ISBN 978-3-031-31422-3. https://doi.org/10.1007/978-3-031-31423-0, xxi+294 pages.
7. P. Hauret and P. Le Tallec. Energy-controlling time integration methods for nonlinear elastodynamics and low-velocity impact. *Computer Methods in Applied Mechanics and Engineering*, 195(37-40):4890–4916, 2006.
8. H. M. Hilber, T. J. Hughes, and R. L. Taylor. Improved numerical dissipation for time integration algorithms in structural dynamics. *Earthquake Engineering & Structural Dynamics*, 5(3):283–292, 1977.
9. H. Huang, N. Pignet, G. Drouet, and F. Chouly. HHT-α and TR-BDF2 schemes for dynamic contact problems. *Computational Mechanics*, 2023. https://doi.org/10.1007/s00466-023-02405-9.
10. H. B. Khenous, P. Laborde, and Y. Renard. Mass redistribution method for finite element contact problems in elastodynamics. *European Journal of Mechanics-A/Solids*, 27(5):918–932, 2008.
11. J. Nitsche. Über ein variationsprinzip zur lösung von dirichlet-problemen bei verwendung von teilräumen, die keinen randbedingungen unterworfen sind. In *Abhandlungen aus dem mathematischen Seminar der Universität Hamburg*, volume 36, pages 9–15. Springer, 1971.
12. Y. Renard and K. Poulios. GetFEM: Automated FE modeling of multiphysics problems based on a generic weak form language. *ACM Transactions on Mathematical Software (TOMS)*, 47(1):1–31, 2020.